Enabling the Assimilation of CrIS Shortwave Infrared Observations in Global NWP at NOAA. Part I: Background and Methods

ERIN JONES,[a,b,c] KEVIN GARRETT,[d] KAYO IDE,[b] YINGTAO MA,[c,e] BRYAN KARPOWICZ,[f,g] CHRISTOPHER BARNET,[h] AND SID BOUKABARA[i]

[a] *University of Maryland CISESS, College Park, College Park, Maryland*
[b] *University of Maryland Earth System Science Interdisciplinary Center, College Park, College Park, Maryland*
[c] *NOAA/NESDIS Center for Satellite Applications and Research, College Park, College Park, Maryland*
[d] *NOAA/NWS Office for Science and Technology Integration, Silver Spring, College Park, Maryland*
[e] *Colorado State University CIRA, College Park, College Park, Maryland*
[f] *NASA GMAO, Greenbelt, Maryland*
[g] *University of Maryland, Baltimore County, Baltimore, Maryland*
[h] *Science and Technology Corporation, Columbia, Maryland*
[i] *NASA Earth Science Division, Washington, D.C.*

(Manuscript received 17 October 2023, in final form 10 June 2024, accepted 13 August 2024)

ABSTRACT: Radiance observations from Earth-observing satellites have a significant positive impact on numerical weather prediction (NWP) forecasts, but some spectral regions are not fully exploited. Observations from hyperspectral infrared (IR) sounders in the longwave region (650–1100 cm^{-1}), for instance, are routinely assimilated in many NWP models, but observations in the shortwave region (2155–2550 cm^{-1}) are not. Each of these regions provides information on the temperature structure of the atmosphere, but the shortwave IR (SWIR) region is considered challenging to assimilate due to noise-equivalent delta temperature (NEDT) that is highly variable depending on scene brightness temperature and to phenomena that are difficult to model, like nonlocal thermodynamic equilibrium (NLTE) and solar reflectance. With recent advances in small-satellite technology, SWIR temperature sounders may provide an agile and cost-effective complement to the current constellation of IR sounders. Therefore, a better understanding of the use and impact of SWIR observations in data assimilation for NWP is warranted. In Part I of this study, as presented here, the amount of unique information [as determined by empirical orthogonal decomposition (EOD)] made available to a data assimilation system by Cross-track Infrared Sounder (CrIS) SWIR observations is reviewed, recent advancements to the Community Radiative Transfer Model (CRTM) for the simulation of CrIS shortwave radiances are tested, and enhancements to NOAA's Global Data Assimilation System (GDAS) for the assimilation of CrIS SWIR observations are implemented and evaluated. Part II of this study, which seeks to assess the value of assimilating shortwave IR observations in global NWP, is also introduced.

KEYWORDS: Satellite observations; Numerical weather prediction/forecasting; Data assimilation

1. Introduction

Since the launch of the *Television and Infrared Observation Satellite-1* (*TIROS-1*) in 1960, observations from Earth-observing satellites have become an increasingly important (and an increasingly prevalent) source of information about the Earth–atmosphere system. Though early efforts to ingest data from instruments on board Earth-observing satellites in data assimilation systems to improve the initial states of numerical weather prediction (NWP) models in the late 1960s and the 1970s may have shown modest benefits over limited areas of the globe (Eyre et al. 2020), satellite data now comprise the bulk of the observations ingested into global data assimilation systems and collectively provide the largest impact on global NWP forecasts through the improvements they produce in the data assimilation analysis or the NWP model initial state. Of the satellite data available for use in data assimilation, radiometer observations from passive microwave and hyperspectral infrared (IR) sensors on board low-Earth-orbiting (LEO) and geostationary orbit (GEO) satellites have often been a major focus for research, owing to their ability to provide regular global (as in the case of polar-orbiting LEO satellites) or regional (e.g., GEO satellites) soundings of important atmospheric properties.

At the National Oceanic and Atmospheric Administration (NOAA), LEO hyperspectral IR data from the Atmospheric Infrared Sounder (AIRS) on board the National Aeronautics and Space Administration (NASA) *Aqua* satellite (Aumann et al. 2003), the European Organisation for the Exploitation of Meteorological Satellites (EUMETSAT) Infrared Atmospheric Sounding Interferometer (IASI) on the MetOp series satellites (Chalon et al. 2001), and the Cross-track Infrared Sounder (CrIS) on the *Suomi National Polar-Orbiting Partnership* (*SNPP*), *NOAA-20*, and *NOAA-21*, and the future Joint Polar Satellite System (JPSS) (Han et al. 2013) satellites are (or will be, in the case of the future JPSS missions) used operationally in data assimilation. The use of data from these hyperspectral IR sounders is of particular interest to global data assimilation, owing to the fact that hyperspectral IR data provide valuable information regarding cloud and surface properties, as

Supplemental information related to this paper is available at the Journals Online website: https://doi.org/10.1175/JTECH-D-23-0148.s1.

Corresponding author: Erin Jones, eejones1@umd.edu

DOI: 10.1175/JTECH-D-23-0148.1

well as environmental temperature, moisture, ozone, and other trace gas profiles with high vertical resolution when compared to passive microwave sounders. Additionally, beginning with AIRS, hyperspectral IR data have, like passive microwave data, been routinely shown to have significant impacts on medium-range NWP (Hilton et al. 2012; McCarty et al. 2009). Le Marshall et al. (2005) demonstrated positive impacts on Northern and Southern Hemisphere height anomaly correlations when assimilating clear-sky AIRS longwave IR (LWIR) radiances in the NOAA National Centers for Environmental Prediction (NCEP) Global Forecast System (GFS). Similarly, Mcnally et al. (2006) demonstrated modest improvements in forecast skill when assimilating AIRS in the European Centre for Medium-Range Weather Forecasts (ECMWF) four-dimensional variational data assimilation (4D-Var) system, but showed greater positive impacts in height anomaly correlations when compared to a single Advanced Microwave Sounding Unit-A (AMSU-A) or High Resolution Infrared Radiation Sounder (HIRS) instrument. Later, IASI, with characteristics (e.g., spatial and spectral coverage) similar to AIRS but with improved quality/reduced noise in the LWIR region (Collard and McNally 2009; Hilton et al. 2009), and CrIS were implemented in the operational global data assimilation systems of many NWP centers. The use of IASI and CrIS added both additional spatial coverage to the hyperspectral IR sounder observing system and incremental improvements to NWP forecast skill (Collard et al. 2012; Eresmaa et al. 2017; Smith et al. 2015).

As a result of the efforts to assimilate hyperspectral IR sounding data in global data assimilation systems, hyperspectral IR sounders consistently rank above the median in their overall contributions to NWP forecast error reduction (Dahoui et al. 2017; Lorenc and Marriott 2014) at many NWP centers, when compared to other components of the global observing system. Historically, these efforts have mostly been concentrated on the use of data from the LWIR (specifically temperature channels from ~650 to 1100 cm^{-1} or ~15.385–9.091 μm)—and, to a lesser extent, the midwave IR (MWIR; ~1200–1750 cm^{-1} or ~8.333–5.714 μm)—parts of the spectrum. The methods for assimilating hyperspectral IR sounding data for use in global data assimilation have also typically been similar to those often used for brightness temperature data assimilation: Assimilation has often been limited to clear-sky observations (and therefore requires the use of a cloud detection scheme to remove cloudy and/or precipitating observations) and uses variational bias correction and well-established methods for quality control (e.g., checks for outliers). More recent work, such as the assimilation of more channels with strong sensitivity to water vapor, the use of correlated observation errors, and the use of observations in all-sky conditions, has served to refine the process of assimilating data from hyperspectral IR sounders and to help increase their impact on NWP systems (e.g., Okamoto et al. 2019; Geer 2019; Geer et al. 2019; Okamoto et al. 2023).

Though data from the shortwave IR (SWIR) part of the spectrum have historically been readily available from hyperspectral IR sounders, their use in data assimilation systems has generally not been implemented operationally at NWP centers, and minimal research has been done to explore their use in global data assimilation (e.g., Noh et al. 2021). Up until now, this has largely been due to a lack of solutions to certain challenges that may be encountered when attempting to assimilate SWIR data. While SWIR and LWIR sounding channels have similar vertical sensitivity to atmospheric temperature, the SWIR part of the spectrum is typically associated with higher instrument noise (though the information to noise ratio is similar to that of the LWIR part of the spectrum), which may reduce forecast impacts. SWIR observations may also be sensitive to solar radiation reflecting off the surface, clouds, and aerosols, and stratospheric sounding channels may be sensitive to the effects of nonlocal thermodynamic equilibrium (NLTE). These challenges with solar reflectance and NLTE require more sophisticated radiative transfer modeling, especially during the daytime, to account for these effects during the assimilation process. Additionally, the broader 4-μm region of the SWIR part of the spectrum has sensitivity to trace gas absorbers such as nitrous oxide (N_2O) and carbon monoxide (CO), thereby requiring a better a priori knowledge of their concentrations in the atmosphere, and a better knowledge of their impact on the SWIR observation error covariance, for assimilation of impacted channels to be fully exploited.

Despite the challenges inherent in assimilating SWIR observations from hyperspectral IR sounders, SWIR data can provide potential benefits to a data assimilation system: SWIR channels tend to have a finer vertical resolution than their LWIR counterparts, and the signal for temperature-sensitive SWIR channels typically tends to experience less interference from water vapor, ozone, and other trace gases than similar LWIR channels, owing to a very low sensitivity to these gases when compared to LWIR (Kaplan et al. 1977). On hyperspectral IR sensors that contain SWIR and LWIR bands, the SWIR observations can also provide redundant information to data assimilation systems in the event of problems or failures with the more commonly used LWIR band. Temperature sounding channels from the LWIR band of *SNPP* CrIS have, for instance, routinely been assimilated at NWP centers around the world. The CrIS instrument contains redundant electronics, called "side A" and "side B," to guard against instrument failure, but the LWIR bands on both sides of the instrument have failed (one in June 2021 and the other in August 2023). At the time of writing, the SWIR bands remain available on both sides of the *SNPP* CrIS instrument and, like their LWIR counterparts, provide temperature sounding information that may be used in data assimilation. Barnet et al. (2023) provide a more in-depth discussion of the information available from the CrIS LWIR and SWIR bands.

In potential future satellite observing systems, the appeal of sustaining (e.g., for data gap filling and data gap mitigation) and eventually expanding on current observational capabilities with a cost-effective and agile constellation of IR sounders has brought the possibility of utilizing small satellites (smallsats) that house hyperspectral IR sounders to the forefront of some NOAA next-generation satellite architecture planning strategies. Current technology favors the use of SWIR spectrometers on smallsat platforms, both because these instruments tend to be smaller and lighter than their LWIR counterparts (and tend to have less demand for the power required to support the thermal cooling necessary to prevent the saturation of LWIR bands) and because SWIR instrumentation currently favors producing observations

with smaller fields of view (FOVs), thereby allowing for the higher spatial resolution of observations. The potential use of SWIR instrumentation on these future smallsat platforms makes preparing for the use of, for instance, the previously unassimilated SWIR 4.3-μm carbon dioxide (CO_2) temperature sounding region in global data assimilation and NWP a prudent and advantageous undertaking. This study aims to address the previously mentioned challenges of utilizing SWIR observations from hyperspectral IR sounders and outline the steps taken to achieve a full integration of these SWIR observations in a global data assimilation.

This paper is outlined as follows: Section 2 describes the data used in the study and the information they can provide to a data assimilation system. In section 3, the methodologies employed for assimilating SWIR data are detailed, including quality control, observation error assignment, and forward operator use. A summary of the steps taken to assimilate SWIR data and a short introduction to the next steps taken, which are discussed more thoroughly in Jones et al. (2024, hereafter Part II), are given in section 4.

2. CrIS data

At NOAA, data (mostly LWIR data) from hyperspectral IR sounders CrIS and IASI on board polar-orbiting JPSS and MetOp satellites are currently assimilated operationally in the Global Data Assimilation System (GDAS). These sensors have similar spectral coverage in the SWIR region of the spectrum, though their spectral sampling in the SWIR varies: IASI is sampled at 0.25 cm^{-1}, while CrIS has a spectral sampling of 0.625 cm^{-1}. In this study, only the assimilation of CrIS SWIR observations is considered, mainly due to CrIS's improved instrument performance/noise-equivalent delta temperature (NEDT) over IASI in the SWIR region.

a. Data description

CrIS is a hyperspectral IR interferometer which takes radiance observations over 2211 channels in three spectral bands: the LWIR from 650 to 1095 cm^{-1} (~15.384–9.132 μm, 713 channels), the MWIR from 1210 to 1750 cm^{-1} (~8.264–5.714 μm, 865 channels), and the SWIR from 2155 to 2550 cm^{-1} (~4.640–3.922 μm, 633 channels). Though CrIS data have been available at a nominal spectral resolution (NSR) with varying spectral sampling across these three bands (0.625, 1.25, and 2.5 cm^{-1}, respectively, for LWIR, MWIR, and SWIR), CrIS full spectral resolution (FSR) data, with 0.625 cm^{-1} spectral sampling across all bands, are used in this study. The *SNPP*, *NOAA-20*, and *NOAA-21* satellites, which currently house the CrIS instrument, fly in polar, sun-synchronous orbits, each with equatorial crossing times of around 1330 local time. Each CrIS 2200-km swath contains 30 cross-track fields of regard (FORs), which, owing to the interferometer design, each contain nine FOVs in a 3 × 3 array. At nadir, each individual CrIS FOV has a 14-km footprint, and the overall FOR has a 50-km footprint (at the edge of scan, this footprint is an oval that is ~42 km along the scan line and ~23 km along track). At NOAA–NCEP, LWIR and MWIR observations from both CrIS *SNPP* and *NOAA-20* are assimilated operationally; observations from the SWIR bands of both these instruments are available and ingested in the GDAS for passive monitoring but are not actively assimilated. SWIR observations from these instruments will therefore be used and evaluated in this study, though an emphasis will be placed on CrIS *NOAA-20* since it is currently the primary CrIS instrument.

The CrIS radiances used operationally at NOAA undergo an apodization and a frequency calibration to remove side-lobe contamination and reduce detector-to-detector differences (Barnet et al. 2000). For *SNPP* CrIS, the postcalibration detector differences are around 0.02 K, allowing data assimilation systems the flexibility to select the best FOV for assimilation from scene to scene (Strow et al. 2013). By requirement, the coregistration of the three CrIS focal plane arrays for the LWIR, MWIR, and SWIR bands must be within 1.4% of the FOV diameter to ensure that each band also has consistent geolocation (Han et al. 2013). Although recent work has investigated misalignment between the focal plane arrays, issues manifesting as representativeness errors in data assimilation would likely be isolated to inhomogeneous scenes, such as cloud edges. In practice, this issue is minimal since the SWIR and LWIR bands are being assimilated and assessed separately in this study, with only a few MWIR channels universally used in experiments.

In this study, and operationally at NOAA, a subset of 431 of CrIS's 2211 channels is used in the GDAS (though the full set of 2211 FSR channels is available). This optimized subset of 431 channels has been chosen to represent the independent pieces of information provided by CrIS measurements (Gambacorta and Barnet 2011, 2013; Jung et al. 2017; see the online supplemental material for a specification of the CrIS 431 subset channels). In addition to minimizing data space requirements, this channel subset lessens the computational cost of ingesting and processing CrIS observations in a global data assimilation system and minimizes the impacts of correlated observation errors in situations where these are not accounted for. The 431-channel subset contains 263 CrIS LWIR channels from 661.25 to 1095 cm^{-1} (~15.123–9.132 μm), 103 MWIR channels from 1210 to 1745 cm^{-1} (~8.264–5.731 μm), and 65 CrIS SWIR channels from 2165.625 to 2531.875 cm^{-1} (~4.618–3.950 μm).

b. Information content

One key consideration when gauging the viability of future SWIR hyperspectral sounders is the value and impact that the SWIR has on weather forecasting/situational awareness in general and on global data assimilation in particular. It is therefore necessary to determine whether the SWIR portion of the spectrum has a similar amount of sensitivity to the various gases in the atmospheric column as the LWIR portion of the spectrum most often used in data assimilation, excluding factors which may serve to reduce the signal-to-noise ratio of observations (e.g., instrument noise). In this study, as a starting point to evaluate the use of SWIR observations, information content is considered from a retrieval perspective independent of the data assimilation system and algorithm; see Barnet et al. (2023) for further discussion.

An assessment of the relative information content of SWIR and LWIR bands may be done by examining their respective

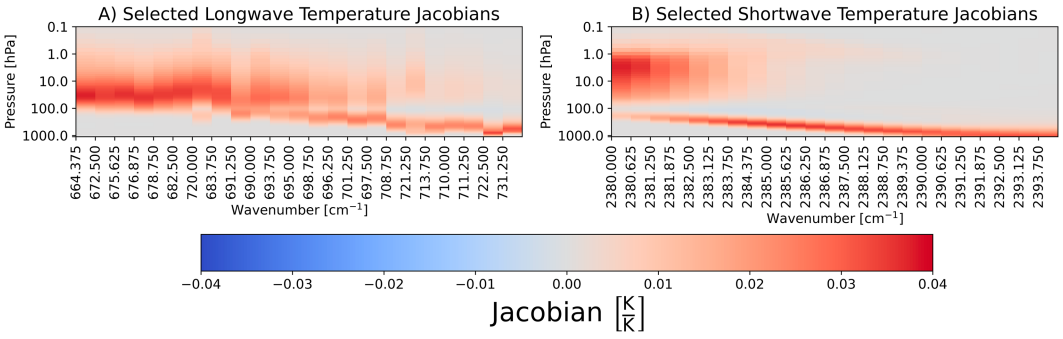

FIG. 1. Temperature Jacobians from the CRTM for a subset of (a) CrIS LWIR channels determined to be near-equivalent to CrIS SWIR *R*-branch channels and (b) CrIS SWIR *R*-branch channels.

temperature Jacobians to ascertain the sensitivities of both SWIR and LWIR sounding channels to temperature. Figure 1 shows the temperature Jacobians of sets of functionally near-"equivalent" (i.e., with similar weighting functions over a series of scenes; see Table 1) LWIR and SWIR channels for a sample clear-sky profile. Note that for upper atmospheric sounding channels [i.e., below 696 cm^{-1} (or ~14.368 μm) in the LWIR and 2383 cm^{-1} (or ~4.196 μm) in the SWIR] there is broad sensitivity to stratospheric temperature. Beyond 696 and 2383 cm^{-1}, the sensitivity moves from the upper troposphere down toward the surface, peaking at about 0.1 K K^{-1} for each band. Though the structure of the temperature Jacobians in the troposphere is similar for LWIR and SWIR channels, the temperature sensitivity for each SWIR channel is concentrated over a smaller vertical range compared to its LWIR counterpart, illustrating the sharper vertical resolution of the SWIR temperature sounding channels. Figure 2 shows the LWIR and SWIR water vapor Jacobians for the same example profile shown in Fig. 1. The SWIR channels can be seen to have reduced sensitivity to water vapor compared to their LWIR counterparts. This lack of sensitivity to water vapor in the SWIR may serve to enhance the temperature signal from SWIR observations.

To further demonstrate the information content of the LWIR and SWIR bands, an empirical orthogonal decomposition (EOD) was performed to compute the eigenvalues for various channel/band combinations from CrIS (see Barnet et al. 2023). The analysis concluded that near-equivalent degrees of freedom (DoFs) were found when comparing the eigenvectors of the SWIR band (~35 DoFs) with those of the 690–790 cm^{-1} (~14.493–12.658 μm) region of the LWIR band (~30 DoFs), the portion of the LWIR band which is

TABLE 1. CrIS SWIR *R*-branch channels and near-equivalent LWIR channels found by comparing weighting functions over a series of clear-sky scenes.

SWIR channel number	SWIR wavenumber	LWIR channel number	LWIR wavenumber
1939	2380.000	24	664.375
1940	2380.625	37	672.500
1941	2381.250	42	675.625
1942	2381.875	44	676.875
1943	2382.500	47	678.750
1944	2383.125	53	682.500
1945	2383.750	115	721.250
1946	2384.375	55	683.750
1947	2385.000	67	691.250
1948	2385.625	65	690.000
1949	2386.250	71	693.750
1950	2386.875	73	695.000
1951	2387.500	79	698.750
1952	2388.125	75	696.250
1953	2388.750	83	701.250
1954	2389.375	77	697.500
1955	2390.000	95	708.750
1956	2390.625	113	720.000
1957	2391.250	103	713.750
1958	2391.875	97	710.000
1959	2392.500	99	711.250
1960	2393.125	117	722.500
1961	2393.750	131	731.250

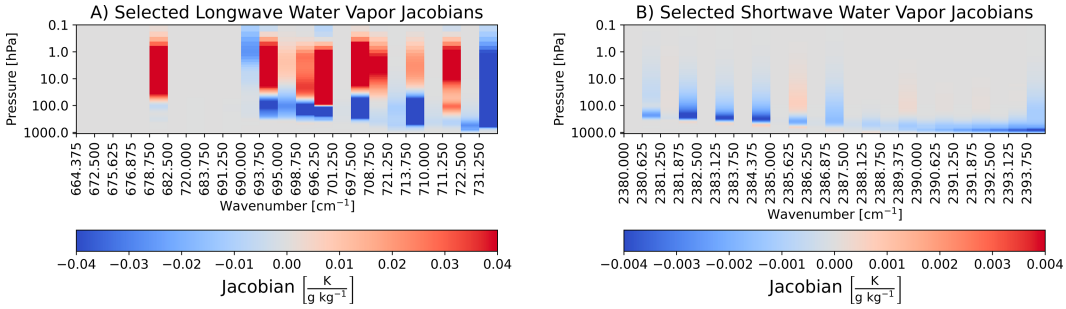

FIG. 2. As in Fig. 1, but for CRTM water vapor Jacobians. Note how the scale in (a) is an order of magnitude greater than the scale in (b), illustrating the difference in sensitivity to water vapor in CrIS SWIR *R*-branch channels and their near-equivalent LWIR channels.

most heavily used in data assimilation and which most closely approximates the temperature sensitivity of the *R* branch, or the high frequency side of the SWIR 4.3-μm CO_2 band (i.e., 2350–2390 cm^{-1} or ~4.255–4.184 μm; as mentioned previously, the temperature sensitivity of this region occurs over less of the vertical column than is seen in the 690–790 cm^{-1} region of the LWIR band, so the DoFs associated with temperature sensitivity in the SWIR *R* branch are more concentrated vertically, allowing for sharper resolution in temperature sounding). Additionally, the performance of EODs that include MWIR channels with LWIR channels (690–790 cm^{-1}) and with SWIR *R*-branch channels show ~65 DoFs for each of the two band combinations [LWIR (690–790 cm^{-1} region) + MWIR and SWIR + MWIR]. This suggests that the use of SWIR observations should have a similar impact on NWP forecast skill that the use of LWIR does, all other factors being equal. A more detailed discussion of this is available in Barnet et al. (2023).

3. Methodology for assimilating shortwave brightness temperatures

The addition of any new observation type to a data assimilation/NWP system not only requires an investigation of the observation's properties (i.e., the amount and nature of the information available) and data quality but also requires an evaluation of the forward operator's ability to represent, or simulate, the observations in the data assimilation system. This assessment of observational data quality and forward model performance is important for the characterization of model and representation errors and the assignment of observation errors. Additionally important is the assessment of any quality control procedures already in place, and the implementation of any new quality control measures necessary for the successful assimilation of the data, and—for SWIR observations—the ability of the radiative transfer model to account for NLTE effects, solar reflection off clouds and the surface, and trace gases (such as N_2O and CO).

a. The forward operator

The CRTM is used for forward and Jacobian calculations in the Gridpoint Statistical Interpolation analysis system (GSI), which serves as the basis of NOAA's GDAS. In NOAA's global NWP system, the Finite-Volume on a Cubed-Sphere GFS (FV3GFS) does not currently provide adequate a priori information regarding N_2O and CO; CrIS SWIR channels sensitive to these trace gases (i.e., those with wavenumbers less than 2270 cm^{-1} or ~4.405 μm) are therefore not considered at this time for evaluation in the CRTM or for assimilation, though channels sensitive to N_2O have the potential to provide temperature sounding information since N_2O, like CO_2, is a well-mixed trace gas with a relatively well-known concentration (Gambacorta and Barnet 2013). Shortward of 2270 cm^{-1}, the CO_2 absorption band (including the *R* branch) can be used to infer the atmospheric temperature profile, but challenges exist in daytime radiative transfer modeling for channels that peak in and above the upper stratosphere. Owing to the low density of air at such altitudes, the assumption of LTE breaks down, primarily in daytime hours: Molecules are heated by the sun to excited states and are unable to redistribute their energy to the surrounding environment through collisions with other molecules, thereby resulting in amplifications of observed brightness temperatures of as much as 10 K, causing the NLTE effect (i.e., the observed brightness temperatures appear warmer than the actual temperature). Since the radiative transfer scheme employed by the CRTM assumes LTE, an additive correction based on the relationship between the differences in LTE and NLTE radiances and two upper atmospheric layer kinetic temperatures was developed by Chen et al. (2013) to address NLTE situations.

Recently, new vibrational temperature (Tvib) profiles are obtained from the Generic Radiative Transfer and NLTE Population Algorithm (GRANADA) with the Michelson Interferometer for Passive Atmospheric Sounding (MIPAS) limb spectra (Jurado-Navarro et al. 2015; Funke et al. 2012; López-Puertas et al. 2009). The newer version of Tvibs includes more solar zenith angles and is based on the upgraded GRANADA model and the newly derived collisional rates. Details and some other improvements can be found in Jurado-Navarro et al. (2015). The NLTE correction in CRTM has been updated with these new Tvib profiles. Figure 3 shows the difference between daytime observed and CRTM simulated [using ECMWF analyses as input, with a bidirectional reflectance distribution function (BRDF, to be discussed later) considered in the simulation] *SNPP* CrIS brightness temperatures. The curves

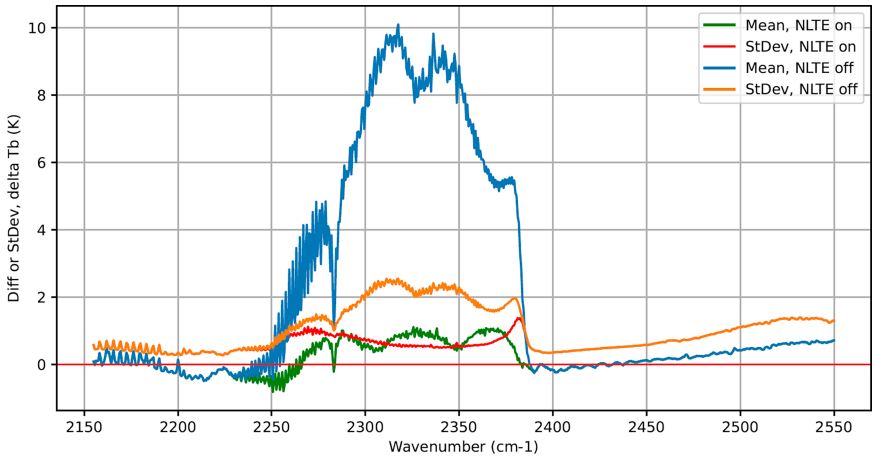

FIG. 3. Statistics of differences [observed minus simulated from analysis fields (OmAs); K] in observed brightness temperatures and CRTM simulated brightness temperatures (simulated, with BRDF applied, from an ECMWF analysis) for clear-sky *SNPP* CrIS SWIR channels. Mean and standard deviation (blue and orange lines, respectively) for OmAs from ~81 000 observations when NLTE correction in the CRTM is turned off, and mean and standard deviation (green and red lines, respectively) when CRTM's NLTE correction is in use for SWIR channels with wavenumbers less than 2390 cm^{-1}. The application of the NLTE correction decreases mean OmAs for impacted channels by as much as 9 K and decreases the standard deviation for OmAs for impacted channels by up to ~2 K.

show the mean and standard deviation of this difference with and without CRTM's NLTE correction applied. When the NLTE correction is not used, large differences (up to 8–10 K or more) are seen between observed and simulated brightness temperatures for wavenumbers between 2250 and 2375 cm^{-1} (~4.444–4.211 μm), and when the NLTE correction is applied, mean differences between observed and simulated brightness temperatures for these wavenumbers are decreased to less than 1.0 K. This remaining bias is consistent with the CRTM's likely underestimation of the NLTE effect, as noted by Chen et al. (2013). The standard deviation of the difference between observed and simulated brightness temperatures is also reduced for channels impacted by NLTE when the NLTE correction is applied. This improved performance allows impacted channels to have more weight in the data assimilation system when they are actively assimilated; the CRTM's NLTE correction for CrIS SWIR is therefore employed in this study. It should be noted that, at the time of writing, the operational version of the CRTM applies an NLTE correction to CrIS SWIR channels with wavenumbers longward of 2400 cm^{-1}; the 2390–2400 cm^{-1} (~4.184–4.167 μm) region, however, is sensitive to lower levels of the atmosphere and should not have an NLTE correction applied. For the sake of this work, consistent with attempting to reproduce the operational setup, the NLTE correction is still applied for these channels (a fix for this is expected to be implemented in a future version of the CRTM).

In addition to NLTE, solar reflectance presents a challenge when modeling SWIR channels with the CRTM. The sun emits IR radiation at wavenumbers that overlap with those in the 4-μm CO_2 band, thereby necessitating that the CRTM account for solar radiation reflected by clouds and Earth's surface when simulating CrIS SWIR observations. Chen et al. (2013) describe the development of a BRDF for SWIR simulation that considers the observation viewing angle, the solar geometry, and the state of the ocean surface (when applicable). Figure 4 illustrates the improvement of a day of CrIS SWIR simulations from the CRTM when the BRDF is enabled and ECMWF analyses are used as input (NLTE is also used). Small improvements (~0.1–0.2 K) in the mean differences between observed and simulated brightness temperatures are noticeable in the 2390–2400 cm^{-1} range, and larger improvements (up to 0.5 K) are seen for lower peaking channels with wavenumbers shortward of 2500 cm^{-1} (4 μm). The standard deviation of the differences between observed and simulated brightness temperatures also improves for the channels shortward of 2390 cm^{-1} that are expected, when actively assimilated, to have the greatest impact on the global forecast and analysis. Along with the NLTE correction, BRDF is also employed in this study.

b. *Cloud detection*

Improvements to the radiative transfer model now make the assimilation of SWIR observations in the GDAS a feasible prospect. These changes alone, however, are not enough to allow for the successful assimilation of data from SWIR channels. The enhancement of existing quality control measures, or the addition of new quality control, is also important for the assimilation of SWIR brightness temperatures. At the time of writing, the versions of FV3GFS used operationally and in this study (v16) assimilate CrIS, and other hyperspectral IR observations, only in clear-sky conditions. To remove cloud-contaminated hyperspectral IR observations, a cloud detection scheme based on Eyre and Menzel (1989) is used operationally to screen for cloudy points. In this scheme, a cloud top pressure p and cloud fraction N are found that minimize

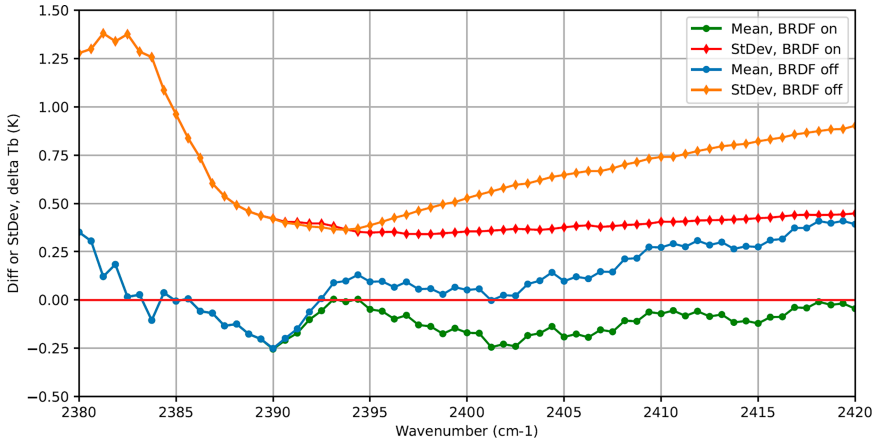

FIG. 4. As in Fig. 3, but showing the mean (blue line) and standard deviation (orange line) of *SNPP* CrIS SWIR OmAs when the CRTM BRDF correction is turned off and the mean (green line) and standard deviation (red line) of these OmAs when the CRTM BRDF correction is turned on. The BRDF correction decreases OmA mean and standard deviation by up to ~1 K for some applicable *SNPP* CrIS SWIR channels. NLTE correction is used in all simulations.

$$\sum \delta^2 = \sum \{(\mathrm{BT}_m - \mathrm{BT}_{\mathrm{clr}}) - N[\mathrm{BT}_{\mathrm{cld}}(p) - \mathrm{BT}_{\mathrm{clr}}]\}^2, \quad (1)$$

where BT_m is the observed brightness temperature, $\mathrm{BT}_{\mathrm{clr}}$ is the clear-sky brightness temperature simulated by the forward model from the background, $\mathrm{BT}_{\mathrm{cld}}(p)$ is the overcast brightness temperature simulated by the forward model at pressure p, and δ is the residual between the observed and simulated clear-sky brightness temperatures. In the GDAS, the summations of Eq. (1) are performed over a set of channels that have been selected for use in the calculation of the cloud profile. The cloud detection scheme iterates through each model level to determine the highest cloud layer and checks all channels against this. If a specific channel's weighting function is determined to peak below the cloud layer at a location, or if more than 2% of the channel's total transmittance is determined to come from the cloud layer, that channel's observation is flagged for cloud at that point and not assimilated.

In the current operational FV3GFS, only CrIS LWIR channels are used to detect cloud for all CrIS observations processed in the GDAS. While this may be appropriate for CrIS MWIR observations, which must rely on CrIS LWIR or SWIR information for cloud detection, using CrIS LWIR channels for cloud detection was determined not to be ideal in this study focused on the use of CrIS SWIR observations when experiments were performed assimilating only CrIS SWIR and operationally used MWIR observations. As discussed previously in section 2b, the SWIR *R* branch has different properties than its LWIR counterpart, including sharper weighting functions throughout the troposphere. A cloud profile produced using LWIR channels would therefore be different than one produced with SWIR channels and may overestimate (or underestimate) cloud. This can be seen in Fig. 5, where cloud amounts are compared for a CrIS SWIR channel when CrIS LW channels and CrIS SWIR channels are used to generate cloud fraction as it would be done in the GDAS for CrIS quality control. The use of CrIS SWIR channels results in noticeably less cloud in many (though not all) regions (see Figs. 5c,d). Additionally, any attempts to use CrIS to approximate a hypothetical hyperspectral IR instrument that contains only SWIR or MWIR and SWIR channels would necessarily require that LWIR channels not be used in cloud detection for clear-sky data assimilation.

c. *Sun glint*

Though the implementation of the BRDF correction in the CRTM has improved the simulation of CrIS SWIR radiances in the daytime, sun glint over water surfaces still presents problems for the radiative transfer model, as can be seen in Fig. 6a, where mean CrIS SWIR uncorrected observation innovations [the difference between observed brightness temperatures and brightness temperatures simulated from the model background or observation minus background (OmBs)] are binned by solar zenith angle and plotted. For some daytime observations (i.e., those with solar zenith angles of less than 90°), errors of over 1 K can be seen in the simulated brightness temperatures. A solution to this issue that is currently employed in the operational GDAS is to deweight or remove all SWIR observations that are taken over water in daytime hours, but this solution does not account for the fact that daytime SWIR observations are not equally impacted by sun glint; the effects of glint vary depending on channel and location.

As it is known where CrIS SWIR observations are most impacted by sun glint, it is possible to isolate these observations and remove them from consideration in the assimilation system. To do this, the glint angle or $\mathrm{gl}_{\mathrm{sun}}$ is calculated in radians at each observation location using

$$\mathrm{gl}_{\mathrm{sun}} = \mathrm{acos}[\cos(|\theta_{\mathrm{sat}}|)\cos(\theta_{\mathrm{sun}}) + \sin(|\theta_{\mathrm{sat}}|)\sin(\theta_{\mathrm{sun}})\cos(\varphi_{\mathrm{rel}})], \quad (2)$$

where θ_{sat} is the satellite zenith angle, θ_{sun} is the solar zenith angle, and φ_{rel} is the relative azimuth angle (Chen et al. 2013). The $\mathrm{gl}_{\mathrm{sun}}$ is then converted into degrees, and any observations

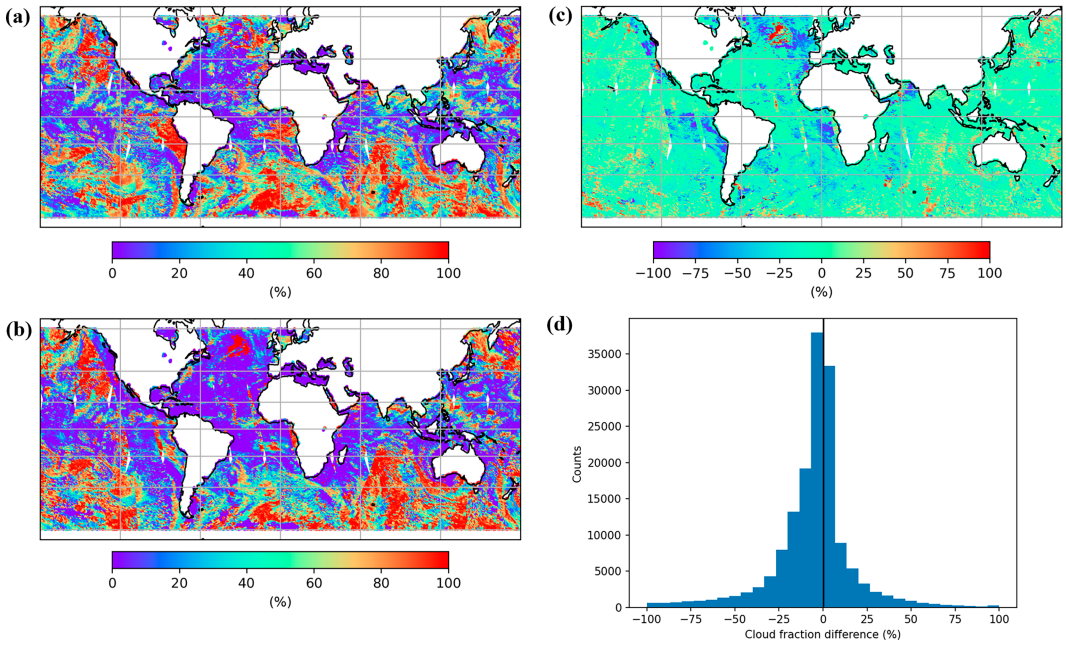

FIG. 5. Cloud fraction calculated using the GDAS cloud detection scheme when (a) CrIS LWIR channels are used and when (b) CrIS SWIR channels are used. (c) Differences in cloud fraction amounts derived from SWIR-based and LWIR-based cloud detection (SWIR cloud fraction minus LWIR cloud fraction) show regions where SWIR-based cloud detection identifies less cloud. (d) This can also be seen in a histogram of SWIR vs LWIR-based cloud fraction differences, where a majority of the distribution is negative.

from channels shortward of 2386.88 cm^{-1} (~4.190 μm) are removed from processing where the calculated glint angle is less than or equal to 15°. When this check for the sun-glint angle is applied, the mean error in simulated brightness temperatures for the most impacted channels is reduced for applicable solar zenith angle ranges, as can be seen in Fig. 6b. A general overview of the quality control measures used for CrIS, and the enhancements made for CrIS SWIR observations, is presented in Table 2.

d. Observation error covariance matrix

The observation error covariance matrix (**R**) is an important component of the data assimilation system, as it serves to determine the weight (or uncertainty) that should be assigned to an observation during the minimization of the four-dimensional ensemble variational (4DEnVar) cost function. The minimization of the cost function provides, given their respective uncertainties, the optimal solution to fit both the background and the observations—in this case, CrIS brightness temperatures. It is therefore important that the observation errors are characterized well. Historically, the **R** matrix for hyperspectral IR instruments has been purely diagonal, but in recent years, many NWP centers have moved toward assimilating hyperspectral IR observations using correlated observation errors (Weston et al. 2014; Bormann et al. 2015). The use of correlated observation errors for hyperspectral IR observations was implemented at NCEP operationally in the FV3GFS in 2021 after Bathmann and Collard (2021) demonstrated forecast improvements when surface-dependent correlated observation errors for CrIS and IASI were used in conjunction with a refined cloud detection algorithm. As the operational data assimilation for hyperspectral IR instruments at NOAA has also been focused largely on the use of LWIR observations, the error covariance matrix for CrIS has not been extended to SWIR channels at the time of writing. Extending the error covariance matrix to SWIR channels, though recommended for future work, was determined to be out of scope for this initial study, since the primary intent was to determine whether the assimilation of SWIR channels is possible [it should be noted, however, that ECMWF has begun exploring this in their system; see Burrows et al. (2023)]. Uncorrelated observation errors were accordingly used for CrIS SWIR in this study, but attempts still needed to be made to more appropriately assign observation errors for SWIR observations. The diagonal values of the **R** matrix therefore needed to be characterized for CrIS SWIR channels.

At present, CrIS SWIR channels are assigned initial observation errors of 1 K in the GDAS, and though these observation errors are modified slightly from scene to scene depending on how likely the observation is to be impacted by cloud, they remain largely static across the model domain. This method for calculating the **R** may be appropriate for LWIR channels, where observation uncertainty varies little from scene to scene, but this is not the case for the SWIR part of the spectrum. Observed CrIS radiances are converted to brightness temperatures prior to being assimilated in the GDAS, and the nonlinearity of the Planck function in the SWIR region can lead to a large error in brightness temperature given a small error in the observed radiance, especially in cold scenes. Though this would not be a

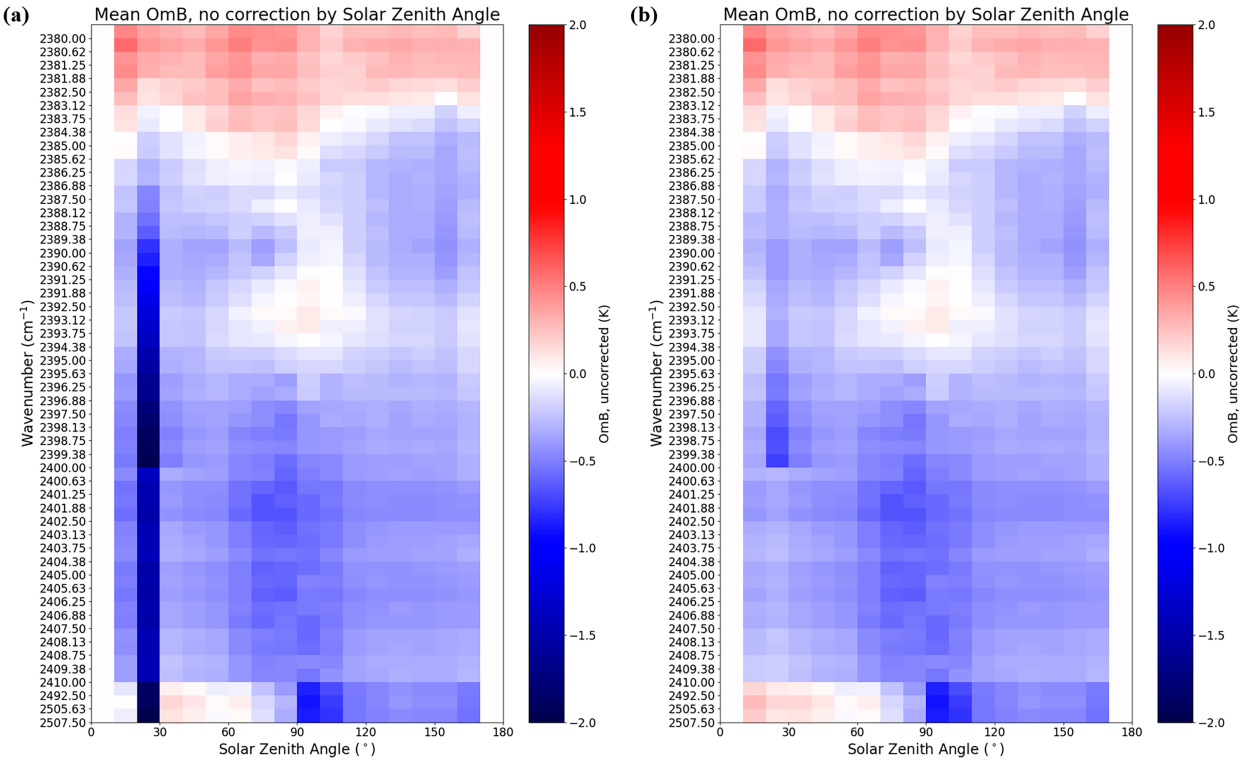

FIG. 6. Average OmB profiles (before bias correction) binned by solar zenith angle for *NOAA-20* CrIS SWIR channels from a day, 15 Dec 2018, in the GDAS. (a) Observations have quality control applied, except for a sun-glint check. Average uncorrected OmBs of less than −1 K can be seen for lower peaking channels during the daytime in a very limited range of solar zenith angles. (b) The sun-glint check is applied in addition to other quality control measures.

challenge if infrared data assimilation were performed using observed radiances instead of brightness temperatures, the use of brightness temperatures therefore introduces additional noise that must be accounted for in the SWIR. To address this, a scene-dependent observation error for those CrIS SWIR channels that are typically colder and higher peaking has been implemented in the GDAS. In this study, for the CrIS SWIR channels longward of 2386 cm^{-1} (~4.191 μm), this observation error σ^o is determined by

$$\sigma^o = \sqrt{\left\{\mathrm{NEDN}(T_{\mathrm{ref}})\middle/\left[\frac{dB(T)}{dT}\right]\right\}^2 + \alpha^2}, \qquad (3)$$

where $dB(T)/dT$ is the derivative of the Planck function at the scene brightness temperature T; NEDN(T_{ref}) is the noise-equivalent delta radiance at a reference brightness temperature (in this study, 280 K) given the instrument error for that channel in question; and α is an added inflation (0.5 K in this study) to account for additional errors, e.g., errors in the forward model and interchannel correlations (which are largely due to the apodization of the data and most strongly impact adjacent channels). The resulting error distribution, as seen in Fig. 7, bears more resemblance to the instrument noise for the channel than the errors that would be used in the GDAS without the implementation of a scene-dependent observation error. Without the implementation of a scene-dependent

TABLE 2. General quality control procedures in the GDAS for CrIS observations and the associated enhancements for SWIR CrIS observations. Not included here are rudimentary checks on the data for physicality, date/time applicability, realistic geolocation assignments, checks that the channel should be processed, or checks that the CRTM was able to simulate the observation without error.

Quality control for CrIS observations	
General QC procedure	SWIR enhancement
Gross check	No change to gross check
LWIR-based cloud detection	Use SWIR channels for SWIR cloud detection
LWIR-based skin temperature sensitivity check	Use SWIR channels for SWIR skin temperature sensitivity check
Additional skin temperature sensitivity check over land	No change to skin temperature sensitivity check over land
SWIR only: check for observations over water in daytime	Observations from SWIR channels shortward of 2386.88 cm^{-1} that are sensitive to glint are removed

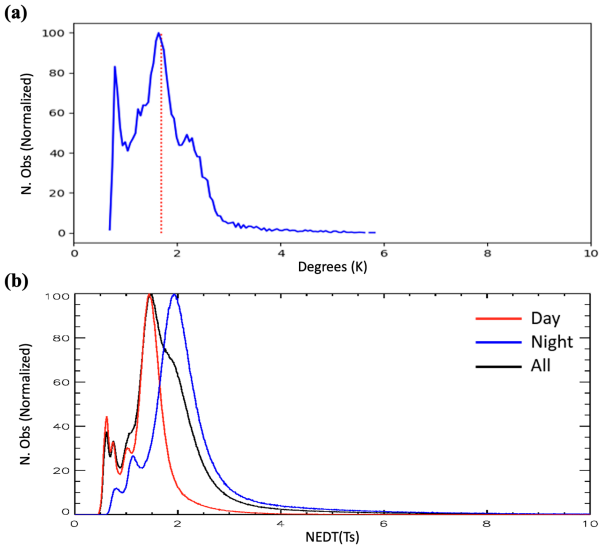

FIG. 7. Sample histograms (with the number of observations normalized by the number of observations in the largest bin) of observation errors for CrIS SWIR channel 1939 (2380 cm^{-1}) from (a) the GDAS when a scene-dependent observation error is applied and (b) the actual instrument noise (NEDT). The lack of variability in the observation error is not applied and is not shown here, but the distribution has a standard deviation of 0.012 K. When the scene-dependent error is applied, the sample standard deviation increases to 0.648 K, illustrating the increased variability in the observation error with the implementation of scene dependency.

observation error, the observation error in the GDAS is nearly static for many CrIS SWIR channels [e.g., the observation error distribution at 2380 cm^{-1} (~4.202 μm) has a standard deviation of 0.012 K], despite the OmB distribution for these channels often being broad [e.g., the standard deviation for the OmB distribution (not shown here) of observations that pass quality control at 2380 cm^{-1} is about 0.94 K]. With the implementation of the scene-dependent error, the observation error distribution is broad, non-Gaussian, and with a long tail at the high end of the distribution (which is indicative of the presence of a range of cold observations in the sample). This use of the scene-dependent observation error in some CrIS SWIR channels (i.e., those that are colder and higher peaking) allows for those observations taken in warmer conditions to be weighted more heavily in the analysis while still appropriately deweighting observations that are known to be taken in colder scenes and have higher error. Figure 8 shows a two-dimensional depiction of this scene-dependent observation error for the descending orbits of CrIS wavenumber 2380 cm^{-1} from a day in the Northern Hemisphere winter. Observation errors range from less than 1 K in the polar regions to over 3 K in the tropics, illustrating how the observation error increases as the tropopause height increases and the scene brightness temperature decreases. It should be noted that while the focus here is on using a scene-dependent observation error for some CrIS SWIR channels, all channels from CrIS (and other hyperspectral IR sensors) would benefit from the use of an error that varies with scene brightness

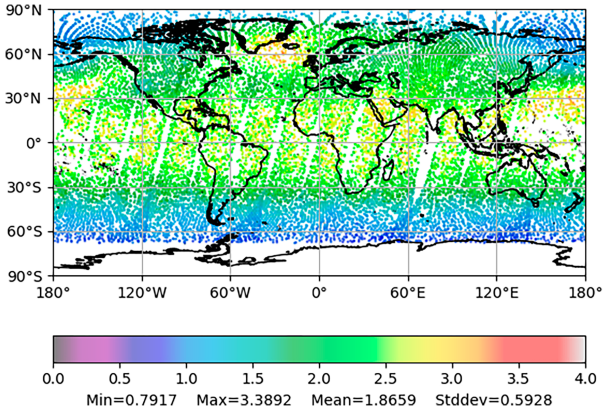

FIG. 8. GDAS observation errors for *NOAA-20* CrIS channel 1939 (2380 cm^{-1}) for descending orbits on 1 Jan 2019 with a scene-dependent error applied. Higher errors are apparent where tropopause height is greater, and tropopause temperatures are therefore colder.

temperature, but the investigation of the use of a scene-dependent error for LWIR and MWIR channels was out of the scope of this study.

4. Summary and next steps

In the first part of this study, the rationale for investigating the viability for assimilating CrIS SWIR observations was discussed, as were the required changes that were implemented in the CRTM and the GDAS. The CrIS SWIR band contains channels (the SWIR *R* branch) that are highly sensitive to atmospheric temperature and largely free of interference from water vapor, ozone, and other trace gases. These channels also have sharper weighting functions than their LWIR counterparts, suggesting that CrIS SWIR channels have sounding capabilities at a better vertical resolution than near-equivalent CrIS LWIR channels. Additional analysis presented by Barnet et al. (2023) shows that, when considering the CrIS 431-channel subset ingested operationally in NOAA's global data assimilation system, the amount of information available from CrIS SWIR channels is similar to the amount of information provided to the GDAS by the portion of the CrIS LWIR band most heavily used in data assimilation at NOAA and that retrievals performed using observations from these two bands show comparable results.

In the past, limitations in radiative transfer models were barriers to using SWIR observations from CrIS (and other hyperspectral IR sensors) in data assimilation, as it was difficult to accurately simulate these observations due to solar and NLTE effects, but BRDF and NLTE corrections have been implemented in radiative transfer models in recent years. Such advancements in the CRTM have been shown to improve the simulation of CrIS SWIR observations in the daytime, thereby also improving the OmB statistics from applicable CrIS SWIR channels. This suggests that making attempts to assimilate these observations in the GDAS is now feasible from a radiative transfer standpoint. Improvements made to the CRTM,

enhancements made to GDAS quality control for cloud and sun-glint detection for SWIR observations, and the implementation of a scene-dependent observation error were all necessary modifications to the GDAS to allow for the use of CrIS SWIR observations. Including these modifications improved observation innovation statistics for CrIS SWIR and therefore served to make it possible to demonstrate the assimilation of CrIS SWIR observations in a global system.

Upon the testing of CRTM NLTE and BRDF corrections and the implementation of SWIR enhancements in the data assimilation system, the next step was to perform a series of observing system experiments (OSEs) to test the impacts of CrIS SWIR assimilation on GDAS analyses and FV3GFS forecasts. An additional intent was to assess the feasibility of the use of a hyperspectral IR instrument with no LWIR channels in data assimilation for global NWP, as current cubesat/smallsat platforms and the demand for observations with higher spatial resolution would likely favor the housing of SWIR or SWIR/MWIR sensors. The setup and results of the OSEs performed to test the assimilation of CrIS SWIR data are discussed in Part II of this study. Based on OSE findings, recommendations were noted for work that could be done to continue to improve the assimilation of SWIR observations from CrIS and other sensors, and these are also discussed.

Acknowledgments. This study was supported by the NOAA/NESDIS Office of Projects, Planning and Acquisition Technology Maturation Program through NOAA Grants NA14NES4320003 (Cooperative Institute for Climate and Satellites) and NA19NES4320002 (Cooperative Institute for Satellite Earth System Studies) at the University of Maryland Earth System Science and Interdisciplinary Center. The authors would like to acknowledge Nadia Smith for her guidance and contributions and Chris Burrows and Tony McNally (and others) at ECMWF for their collaboration. The authors would additionally like to thank Steven Pawson for his encouragement in this work and for funding provided by NASA's Modeling Analysis and Prediction (MAP) to allow for its publication.

Data availability statement. The NWP forecasts, analyses, and associated data upon which this study is based are too large to publicly host and transfer. To reproduce experiments, the forecast model and data assimilation system codes are available on GitHub at https://github.com/ufs-community/ufs-weather-model for the FV3GFS (GFS.v16.0.16 tag) and https://github.com/NOAA-EMC/GSI.git for the GDAS (gfsda.v16.1.4 tag). The code changes to the data assimilation system that were used in this study are available on GitHub (https://github.com/erinjones2/GSI). The exact global workflow used to cycle the forecasts and analyses in study experiments is no longer available, but was previously located in a branch labeled "feature/ops-orion" on the NOAA Environmental Modeling Center's (EMC's) global workflow github (https://github.com/NOAA-EMC/global-workflow) and was tailored to be as close as possible to the global workflow used in operations at the time experiments were being performed (i.e., 2021–22) while allowing for updates required to run the system on the Orion supercomputer operated by Mississippi State University. Experiments in this study were run from initial conditions and observational data archived on NOAA's tape archive. Due to privacy restrictions, not all data are publicly available. More information on these data and how to request access can be found at https://www.nco.ncep.noaa.gov/pmb/docs/restricted_data/.

REFERENCES

Aumann, H. H., and Coauthors, 2003: AIRS/AMSU/HSB on the Aqua mission: Design, science objectives, data products, and processing systems. *IEEE Trans. Geosci. Remote Sens.*, **41**, 253–264, https://doi.org/10.1109/TGRS.2002.808356.

Barnet, C. D., J. M. Blaisdell, and J. Susskind, 2000: Practical methods for rapid and accurate computation of interferometric spectra for remote sensing applications. *IEEE Trans. Geosci. Remote Sens.*, **38**, 169–183, https://doi.org/10.1109/36.823910.

——, N. Smith, K. Ide, K. Garrett, and E. Jones, 2023: Evaluating the value of CrIS shortwave-infrared channels in atmospheric-sounding retrievals. *Remote Sens.*, **15**, 547, https://doi.org/10.3390/rs15030547.

Bathmann, K., and A. Collard, 2021: Surface-dependent correlated infrared observation errors and quality control in the FV3 framework. *Quart. J. Roy. Meteor. Soc.*, **147**, 408–424, https://doi.org/10.1002/qj.3925.

Bormann, N., M. Bonavita, R. Dragani, R. Eresmaa, M. Matricardi, and T. McNally, 2015: Enhancing the impact of IASI observations through an updated observation error covariance matrix. ECMWF Tech. Memo. 756, 56 pp., https://www.ecmwf.int/sites/default/files/elibrary/2015/8292-enhancing-impact-iasi-observations-through-updated-observation-error-covariance-matrix.pdf.

Burrows, C., M. Marticardi, C. Lupu, and T. McNally, 2023: Assimilating short-wave infrared radiances from CrIS at ECMWF. 1 pp., https://itwg.ssec.wisc.edu/wordpress/wp-content/uploads/2023/05/poster.15p.01.Burrows-Chris-Burrows_itsc24.pdf.

Chalon, G., F. Cayla, and D. Diebel, 2001: IASI: An advanced sounder for operational meteorology. *Proc. 52nd Congress of IAF*, Toulouse, France, CNES.

Chen, Y., Y. Han, P. van Delst, and F. Weng, 2013: Assessment of shortwave infrared sea surface reflection and nonlocal thermodynamic equilibrium effects in the community radiative transfer model using IASI data. *J. Atmos. Oceanic Technol.*, **30**, 2152–2160, https://doi.org/10.1175/JTECH-D-12-00267.1.

Collard, A. D., and A. P. McNally, 2009: The assimilation of Infrared Atmospheric Sounding Interferometer radiances at ECMWF. *Quart. J. Roy. Meteor. Soc.*, **135**, 1044–1058, https://doi.org/10.1002/qj.410.

——, J. Derber, and R. Treadon, 2012: Toward assimilation of CrIS and ATMS in the NCEP global model. *18th Int. TOVS Study Conf.*, Toulouse, France, International TOVS Working Group, 1.18, https://itwg.ssec.wisc.edu/conferences/past-itsc-meetings/itsc-18-program.

Dahoui, M., L. Isakssen, and G. Radnoti, 2017: Assessing the impact of observations using observation-minus-forecast residuals. *ECMWF Newsletter*, No. 152, ECMWF, Reading, United Kingdom, 27–31, https://www.ecmwf.int/sites/default/files/elibrary/2017/18195-assessing-impact-observations-using-observation-minus-forecast-residuals.pdf.

Eresmaa, R., J. Letertre-Danczak, C. Lupu, N. Bormann, and A. P. McNally, 2017: The assimilation of Cross-track Infrared Sounder radiances at ECMWF. *Quart. J. Roy. Meteor. Soc.*, **143**, 3177–3188, https://doi.org/10.1002/qj.3171.

Eyre, J. R., and W. P. Menzel, 1989: Retrieval of cloud parameters from satellite sounder data: A simulation study. *J. Appl. Meteor.*, **28**, 267–275, https://doi.org/10.1175/1520-0450(1989)028<0267:ROCPFS>2.0.CO;2.

——, S. J. English, and M. Forsythe, 2020: Assimilation of satellite data in numerical weather prediction. Part I: The early years. *Quart. J. Roy. Meteor. Soc.*, **146**, 49–68, https://doi.org/10.1002/qj.3654.

Funke, B., M. López-Puertas, M. García-Comas, M. Kaufmann, M. Höpfner, and G. P. Stiller, 2012: GRANADA: A generic radiative transfer and non-LTE population algorithm. *J. Quant. Spectrosc. Radiat. Transfer*, **113**, 1771–1817, https://doi.org/10.1016/j.jqsrt.2012.05.001.

Gambacorta, A., and C. Barnet, 2011: Methodology and information content of the NOAA NESDIS operational channel selection for the Cross-track Infrared Sounder (CrIS). NOAA Tech. Rep. NESDIS 133, 36 pp., https://repository.library.noaa.gov/view/noaa/1272.

——, and C. D. Barnet, 2013: Methodology and information content of the NOAA NESDIS operational channel selection for the Cross-track Infrared Sounder (CrIS). *IEEE Trans. Geosci. Remote Sens.*, **51**, 3207–3216, https://doi.org/10.1109/TGRS.2012.2220369.

Geer, A. J., 2019: Correlated observation error models for assimilating all-sky infrared radiances. *Atmos. Meas. Tech.*, **12**, 3629–3657, https://doi.org/10.5194/amt-12-3629-2019.

——, S. Migliorini, and M. Matricardi, 2019: All-sky assimilation of infrared radiances sensitive to mid- and upper-tropospheric moisture and cloud. *Atmos. Meas. Tech.*, **12**, 4903–4929, https://doi.org/10.5194/amt-12-4903-2019.

Han, Y., and Coauthors, 2013: Suomi NPP CrIS measurements, sensor data record algorithm, calibration and validation activities, and record data quality. *J. Geophys. Res. Atmos.*, **118**, 12 734–12 748, https://doi.org/10.1002/2013JD020344.

Hilton, F., N. C. Atkinson, S. J. English, and J. R. Eyre, 2009: Assimilation of IASI at the Met Office and assessment of its impact through observing system experiments. *Quart. J. Roy. Meteor. Soc.*, **135**, 495–505, https://doi.org/10.1002/qj.379.

——, and Coauthors, 2012: Hyperspectral Earth observation from IASI: Five years of accomplishments. *Bull. Amer. Meteor. Soc.*, **93**, 347–370, https://doi.org/10.1175/BAMS-D-11-00027.1.

Jones, E., K. Garrett, K. Ide, B. Karpowicz, C. Barnet, Y. Ma, and S. Boukabara, 2024: Enabling the assimilation of CrIS shortwave infrared observations in global NWP at NOAA. Part II: OSEs and results. *J. Atmos. Oceanic Technol.*, **41**, 1277–1295, https://doi.org/10.1175/JTECH-D-23-0149.1.

Jung, J. A., A. Collard, K. Bathmann, D. Groff, A. Heidinger, and M. Goldberg, 2017: Preparing for CrIS full spectral resolution radiances in the NCEP Global Forecast System. *Proc. 21st Int. TOVS Study Conf.*, Darmstadt, Germany, International TOVS Working Group, 9p.02, https://cimss.ssec.wisc.edu/itwg/itsc/itsc21/program/posters/9p.02_jung.pdf.

Jurado-Navarro, Á. A., M. López-Puertas, B. Funke, M. García-Comas, A. Gardini, G. P. Stiller, and T. von Carlmann, 2015: Vibrational-vibrational and vibrational-thermal energy transfers of CO_2 with N_2 from MIPAS high-resolution limb spectra. *J. Geophys. Res. Atmos.*, **120**, 8002–8022, https://doi.org/10.1002/2015JD023429.

Kaplan, L. D., M. T. Chahine, J. Susskind, and J. E. Searl, 1977: Spectral band passes for a high precision satellite sounder. *Appl. Opt.*, **16**, 322–325, https://doi.org/10.1364/AO.16.000322.

Le Marshall, J., and Coauthors, 2005: Impact of atmospheric infrared sounder observations on weather forecasts. *Eos, Trans. Amer. Geophys. Union*, **86**, https://doi.org/10.1029/2005EO110002.

López-Puertas, M., and Coauthors, 2009: Measurements of polar mesospheric clouds in infrared emission by MIPAS/ENVISAT. *J. Geophys. Res.*, **114**, D00107, https://doi.org/10.1029/2009JD012548.

Lorenc, A. C., and R. T. Marriott, 2014: Forecast sensitivity to observations in the Met Office Global numerical weather prediction system. *Quart. J. Roy. Meteor. Soc.*, **140**, 209–224, https://doi.org/10.1002/qj.2122.

McCarty, W., G. Jedlovec, and T. L. Miller, 2009: Impact of the assimilation of Atmospheric Infrared Sounder radiance measurements on short-term weather forecasts. *J. Geophys. Res.*, **114**, D18122, https://doi.org/10.1029/2008JD011626.

Mcnally, A. P., P. D. Watts, J. A. Smith, R. Engelen, G. A. Kelly, J. N. Thépaut, and M. Matricardi, 2006: The assimilation of AIRS radiance data at ECMWF. *Quart. J. Roy. Meteor. Soc.*, **132**, 935–957, https://doi.org/10.1256/qj.04.171.

Noh, Y.-C., H.-L. Huang, and M. D. Goldberg, 2021: Refinement of CrIS channel selection for global data assimilation and its impact on the global weather forecast. *Wea. Forecasting*, **36**, 1405–1429, https://doi.org/10.1175/WAF-D-21-0002.1.

Okamoto, K., Y. Sawada, and M. Kunii, 2019: Comparison of assimilating all-sky and clear-sky infrared radiances from Himawari-8 in a mesoscale system. *Quart. J. Roy. Meteor. Soc.*, **145**, 745–766, https://doi.org/10.1002/qj.3463.

——, T. Ishibashi, and I. Okabe, 2023: All-sky infrared radiance assimilation of a geostationary satellite in the Japan Meteorological Agency's global system. *Quart. J. Roy. Meteor. Soc.*, **149**, 2477–2503, https://doi.org/10.1002/qj.4516.

Smith, A., N. Atkinson, W. Bell, and A. Doherty, 2015: An initial assessment of observations from the Suomi-NPP satellite: Data from the Cross-track Infrared Sounder (CrIS). *Atmos. Sci. Lett.*, **16**, 260–266, https://doi.org/10.1002/asl2.551.

Strow, L. L., and Coauthors, 2013: Spectral calibration and validation of the Cross-track Infrared Sounder on the Suomi NPP satellite. *J. Geophys. Res. Atmos.*, **118**, 12 486–12 496, https://doi.org/10.1002/2013JD020480.

Weston, P. P., W. Bell, and J. R. Eyre, 2014: Accounting for correlated error in the assimilation of high-resolution sounder data. *Quart. J. Roy. Meteor. Soc.*, **140**, 2420–2429, https://doi.org/10.1002/qj.2306.